Available online at www.sciencedirect.com
SCIENCE DIRECT®
C. R. Physique 6 (2005) 977–996
COMPTES RENDUS PHYSIQUE
http://france.elsevier.com/direct/COMREN/

Spintronics/Spintronique

Development of new materials for spintronics

Joël Cibert [a,*], Jean-François Bobo [b], Ulrike Lüders [b]

[a] *Laboratoire Louis-Néel, CNRS, 38042 Grenoble cedex 09, France*
[b] *LNMH CNRS-ONERA, 2, avenue Édouard-Belin, 31400 Toulouse, France*

Available online 2 December 2005

Abstract

This article presents a review of the state of the art of materials used in spintronics. It is devoted to materials exhibiting novel and exciting electronic properties: manganites, double perovskites, spinel ferrites and diluted magnetic semiconductors. We present the main features of these classes of materials as well as the most important solid state physics results obtained from them in the field of spintronics. ***To cite this article: J. Cibert et al., C. R. Physique 6 (2005).***

Résumé

Développement de nouveaux matériaux pour la spintronique. Nous présentons ici une revue de l'état de l'art actuel en matière de recherche fondamentale sur les matériaux pour la spintronique. L'article est essentiellement dédié aux matériaux présentant de nouvelles propirétés électroniques : les manganites, les doubles pérovskites, les ferrites spinelles et les semiconducteurs magnétiques dilués. Pour chacune de ces classes de matériaux, nous présenterons les principales caractéristiques ainsi que les plus importants résultats obtenus par leur aide dans le domaine de la spintronique et de la physique du solide. ***Pour citer cet article : J. Cibert et al., C. R. Physique 6 (2005).***

Keywords: Spintronics; Magnetic semiconductors; Manganites; Perovskites; Ferrites; Spin filtering; Half metal

Mots-clés : Electronique de spin ; Semiconducteurs magnétiques ; Manganites ; Perovskite ; Ferrites ; Filtre à spin ; Demi-métal

Version française abrégée

Cet article présente les dernières avancées en termes de recherche sur les matériaux pour l'électronique de spin. L'accent sera principalement mis sur les matériaux présentant des propriétés électroniques innovantes (forte polarisation de spin, coexistence entre magnétisme et état semiconducteur, propriétés de transport ajustables à la demande entre le comportement isolant et l'état métallique, forte magnétorésistance). Ces matériaux sont essentiellement des oxydes ou des covalents. Dans l'ordre, seront abordés les manganites, les doubles pérovskites, les ferrites et enfin les semiconducteurs magnétiques.

* Corresponding author.
E-mail addresses: joel.cibert@grenoble.cnrs.fr (J. Cibert), jfbobo@onecert.fr (J.-F. Bobo), uluders@onecert.fr (U. Lüders).

1631-0705/$ – see front matter
doi:10.1016/j.crhy.2005.10.008

1. Introduction

Research in the field of spintronics is presently very active, as well in the field of fabrication of novel heterostructures and nanostructures, as in the field of the synthesis of new materials, mostly in thin films, presenting characteristics required for spintronics (magnetic order, large spin polarization, tunable electronic and magnetic characteristics...).

The aim of this article is to provide an overview of the present state of the art in the domain of the preparation of such new materials. We will emphasize the new results obtained with each class of materials. The families of new materials for spintronics presented here are limited to materials with exceptional electronic properties, namely manganites, ferrites, diluted magnetic semiconductors.

2. Magnetic oxydes

2.1. Conducting perovskite manganites: the prototype of the 100% spin-polarized material

Since the fifties, mixed valence manganese oxides, the so-called manganites, have appealed interest and curiosity of the scientific community. This is due to the large variety of their physical properties. Among their properties the ones that interest the spintronics community is the colossal magnetoresistance and the large spin polarization.

In their generic form, manganites have the chemical formula $A_{1-x}A'_xMnO_3$ with A a trivalent rare earth such as La^{3+}, Pr^{3+}, Nd^{3+}, ... and A′ a divalent alkaline cation like Sr^{2+}, Ca^{2+}, Ba^{2+}, ...

The starting compound is of type $AMnO_3$ into which A sites are substituted by A′ ions. x represents the A′ doping, and according to the x value, the manganese mean valence, comprised between Mn^{3+} and Mn^{4+}, is Mn^{3+x}. This value is obtained for an oxygen stoichiometry of O_3 and may vary depending on the preparation conditions of the material.

The crystalline structure of manganites is based on the perovskite unit cell ABO_3. Ideally, it can be considered as a cubic structure like $SrTiO_3$ and named $E2_1$. This structure may be described either as one with B atoms located at the corners of the cube, A atom sitting at the center of the cube and O atomic sites are the middle of the 12 cube edges or as A atoms at the 8 corners of the cube, B atom at the cube center and oxygen atoms on each cube face. This last representation is illustrated in Fig. 1. One can see that B sites, occupied by manganese atoms, have octahedral symmetry with 6 oxygen neighbors. Distortions of this ideal structure are allowed, provided they remain within the tolerance factor t introduced by Goldschmidt [1] and defined by:

$$t = \frac{1}{\sqrt{2}} \frac{r_A + r_O}{r_B + r_O} \tag{1}$$

In the ideal case ($t = 1$), the structure is cubic, for $0.96 < t < 1$, rhomboidal distortions occur and for $t < 0.96$, the distortions are orthorhombic (this is the case for $LaMnO_3$ with $t = 0.95$). These distortions induce a tilt of the MnO_6 octahedrons and a change of the angle of the Mn–O–Mn link. Note that the perovskite structure is stable for $0.89 < t < 1.02$. MnO_6 octahedrons are submitted to another source of strain that affects the Mn–O–Mn distances due to electron–phonon interaction: the Jahn–Teller effect [2,3]. The mechanism of Jahn–Teller effect is related to the influence of tetragonal distortions of MnO_6 octahedrons on the electronic levels of the 3d electrons of Mn^{3+} ions. The five 3d levels of the Mn ion are split into t_{2g} and e_g in octahedral symmetry and Jahn–Teller effect splits e_g doublet and t_{2g} triplet. The gain in electronic energy induces thus a structural strain.

Let us now present the important parameters for the magneto-electronic properties of manganites:

- Mn^{4+} ion doping.
  Electronic and magnetic properties of manganites strongly depend on the ratio of Mn^{3+}/Mn^{4+} controlled by the divalent ion doping x. The T–x phase diagrams of manganites are very rich as shown in Fig. 2.

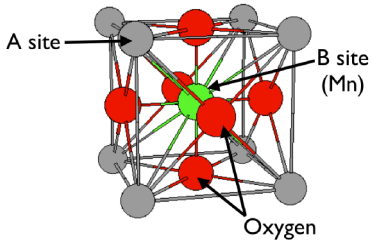

Fig. 1. Representation of the unit cell of manganese perovskite.

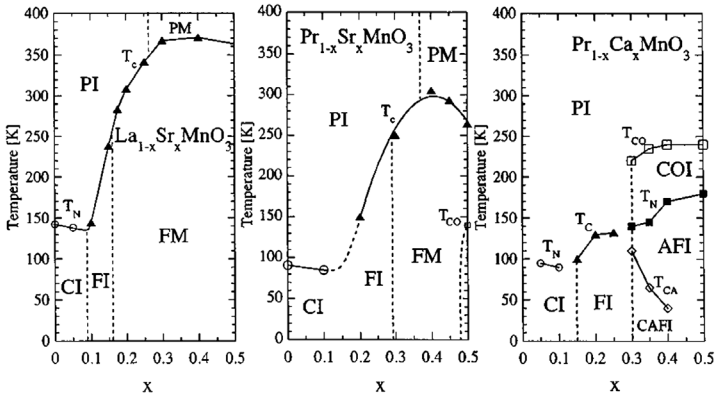

Fig. 2. Phase diagram for perovskite manganites.

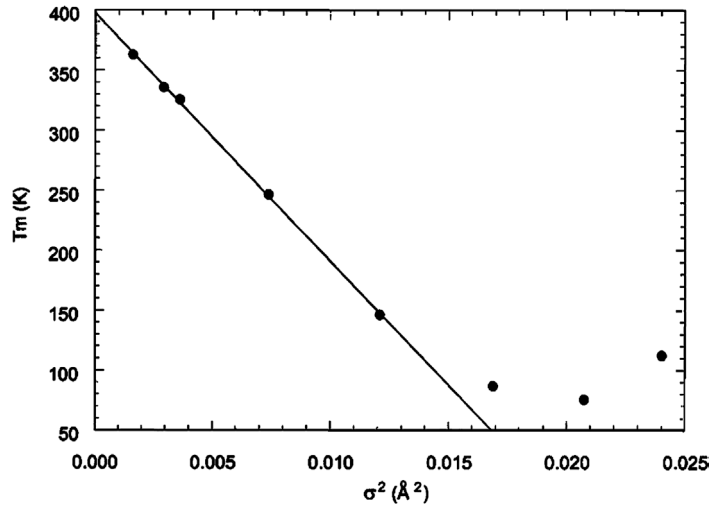

Fig. 3. Influence of ionic radii disorder on the insulating–conducting transition temperature of manganites [5].

- Unit cell deformations.
  Structure plays an important role, mostly through the length and angle of the Mn–O–Mn bond. The overlapping of O p-orbitals and Mn d-orbitals is modified according to the distortions of the unit cell. The importance of these deformations is related to the mean ionic radius $\langle r_A \rangle$ depending on the nature of A and A′ but also on x. Indeed, there are significant differences between the T–x phase diagrams of manganites. For example, with the same doping level ($x = 1/3$), $La_{1-x}Sr_xMnO_3$ and $Nd_{1-x}Sr_xMnO_3$ have Curie temperatures different of 200 K. The difference between the ionic radii of A and A′ cations is also important since it may cause structural disorder and perturb magnetism [4]. Rodriguez-Martinez and Attfield [5] have evidenced a decrease of the insulator–conductor transition temperature for manganites like $A_{0.7}A'_{0.3}MnO_3$ (A = La, Pr, Nd, Sm and A′ = Ca, Sr, Ba) when the ionic radii distribution is more dispersed, the average ionic radius remaining constant (see Fig. 3). Note that the crystal structure is also pressure-dependent leading to metal–insulator transition and increase of the transition temperature with increasing hydrostatic pressure [6,7].
  Finally, oxygen vacancies will also affect the structure: if an oxygen vacancy is present between two manganese ions, their distance will increase, modifying the properties of the material [8,9].
- Temperature and magnetic field.
  The effect of an applied magnetic field on certain manganites is a spectacular decrease of their resistivity which can reach the level of a metal-insulator transition [10,13,18,19]. This magnetoresistive property is the so-called *colossal magnetoresistance* or CMR. Note that the first observation of magnetoresistance in manganites was made in 1969 [11] on the compound $La_{1-x}Pb_xMnO_3$. Such behavior is illustrated in Fig. 4 for an epitaxial $La_{2/3}Sr_{1/3}MnO_3$ thin film [12]. The mechanism of CMR is based on the strong interaction between magnetic order and resistivity in the manganites due to a combination/competition of double exchange (e_g electron hoping is favored if localized magnetic moments of neigh-

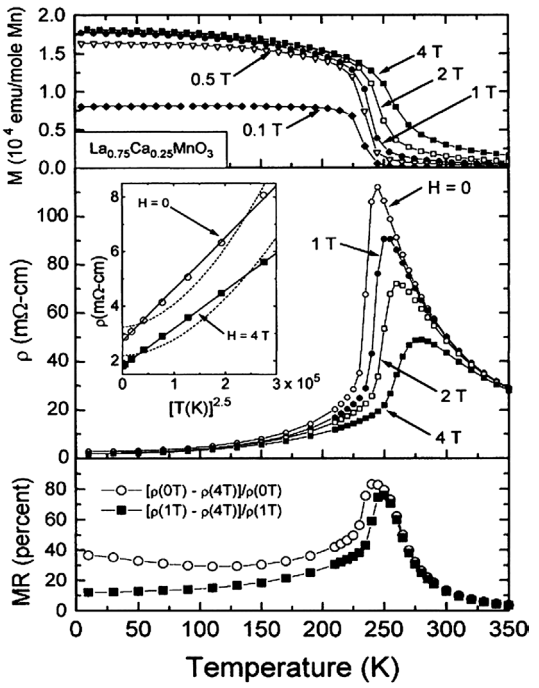

Fig. 4. Observation of colossal magnetoresistance for an epitaxial $La_{2/3}Sr_{1/3}MnO_3$ thin film [12].

bor $Mn^{3+/4+}$ ions are aligned parallel), superexchange (which may cause antiferromagnetic order in some cases) and electron–phonon interaction (related to Jahn–Teller effect). In summary, for conducting ferromagnetic manganites like $La_{2/3}Sr_{1/3}MnO_3$, close to the Curie temperature there is a significant spin disorder that can be suppressed by the application of a magnetic field inducing a large decrease of the material resistivity. In general, several tesla are needed for that (see Fig. 4).

However, manganese perovskites are more famous in spintronics for their large spin polarization and the possibility of making magnetoresistive devices out of them. The first examples were obtained from granular sintered ceramics of manganites. In that case, manganite exhibit *low field magnetoresistance* (LFMR) which does not have the same origin than CMR. Its origin is the tunneling of current between manganite grains whose magnetizations are not aligned parallel to each other (either due to disorder in anisotropy directions or to thermal fluctuations). Extensive study of intergrain magnetoresistance was done by Fontcuberta et al. [14]. Thin film growth progress have allowed to make manganite-based magnetic tunnel junctions. The first results involving manganites in MTJ's were reported by Gupta et al. in 1999 [15]. The observed TMR values are very large (more than 80%), but in order to confirm the total spin polarization of $La_{0.7}Sr_{0.3}MnO_3$ (LSMO), Bowen et al. [16] have prepared optimized MTJ based on two LSMO electrodes separated with a $SrTiO_3$ barrier with very low roughness and intermixing. They could obtain up to 1900% TMR, therefore confirming that the spin polarization of LSMO is larger than 95% (see Fig. 5). However, TMR in perovskite manganites is intrinsically limited by the low Curie temperature of this material. This is even more pronounced for thin films or interfaces, as evidenced by Park et al. [17] (see Fig. 6). This is the main limitation of manganites.

2.2. Double perovskites: challenging materials?

The leading compound of this class of materials is Sr_2FeMoO_6 which is a double perovskite composed of a succession along 3 dimensions of single perovskite unit cells with either Fe^{3+} or Mo^{5+} in the center. Therefore, along the [111] axis, Sr_2FeMoO_6 can be considered like a succession of Fe/O/Sr/O/Mo/O/Sr/O/Fe planes. Fe–O bond length is 1.99 Å while the one of Mo–O bond is 1.96 Å thus favoring a charge transfer from Mo to O. The angle of the Fe–O–Mo trimer is 169°. Sr_2FeMoO_6 structure is quadratic (I4/mmm space group) and its lattice parameters are $a = b = 5.5697$ Å and $c = 7.8986$ Å.

The electronic properties of Sr_2FeMoO_6, instead of being based on the existence of a mixed valence for Mn^{3+}/Mn^{4+} in manganites, depend on the delocalization of the 3d electron of Mo^{5+} ($4d^1$ configuration), leading to the existence of two ionic configurations Mo^{5+}–Fe^{3+} and Mo^{6+}–Fe^{2+} and therefore to the delocalization of one electron. This itinerant electron

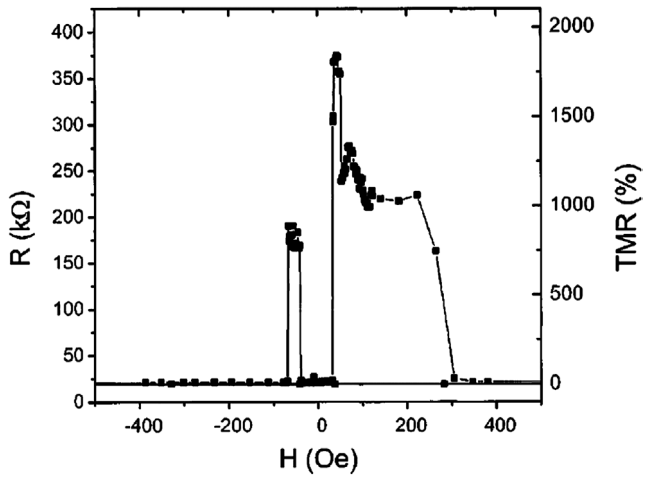

Fig. 5. Observation of extremely high tunnel magnetoresistance on optimized magnetic tunnel junctions [16].

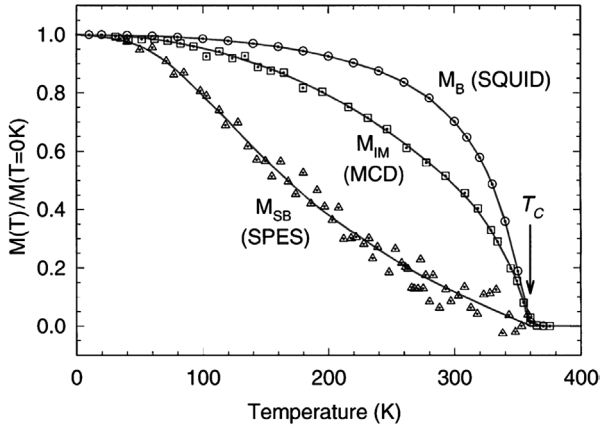

Fig. 6. Temperature dependence of the surface spin polarization (measured by SPES and MCD) and the bulk saturation magnetization for LSMO (measured by SQUID) [17].

is responsible at the same time of the conductivity and the ferrimagnetism in Sr_2FeMoO_6. The overall moment per formula unit is expected to be 4 μ_B. According to bandstructure calculations by Kobayashi et al., Sr_2FeMoO_6 is expected to be a half metal ferromagnet [20]. Another specificity of Sr_2FeMoO_6 is that, due to its double perovskite structure, antisite disorder may occur, iron and molybdenum atoms occupying the wrong positions. This kind of disorder induces a significant loss of saturation magnetization (typically 3 μ_B/f.u. instead of the expected 4 μ_B/f.u. for the ideal compound). Balcells et al. have demonstrated a correlation between the deposition temperature and the antisite disorder and a clear relationship between the fraction of site disorder, the saturation magnetization and the Curie temperature of the compound [21].

A major problem with the growth of thin films of Sr_2FeMoO_6 is the possibility of decomposition into parasite phases like iron oxides or iron precipitates. It has been a challenge to obtain single phase Sr_2FeMoO_6 films until the work of Besse et al. [22] who used Pulsed Laser Deposition (PLD) with a low temperature grown seed layer of Sr_2FeMoO_6 followed by a heating ramp up to the optimum growth temperature during the deposition of the whole SFMO film and avoiding thus the formation of extra phases. Such a preparation procedure allowed the same group to obtain magnetic tunnel junctions based on Sr_2FeMoO_6 electrode, $SrTiO_3$ tunnel barrier and Co counter electrode. The technique used was the one of nanojunctions made by conducting tip atomic force microscopy as furtherly presented in Section 2.4. In Fig. 7, the tunnel magnetoresistance (TMR) response of a structure prepared with a Sr_2FeMoO_6 (SFMO) bottom electrode and a Co top electrode is represented. The maximum TMR value is ∼50%, so, taking into account the spin polarization of cobalt (40%) and the Jullière's formula ($TMR = 2P_{SFMO}P_{Co}/(1 - P_{SFMO}P_{Co})$), we can deduce a spin polarization for Sr_2FeMoO_6 of ∼−85% [22]. Note that the observed sign for P_{SFMO} agrees with bandstructure calculations. However, this kind of experiment was not reproduced by other teams and Sr_2FeMoO_6 remains a material extremely difficult to synthesize in thin films for spintronics.

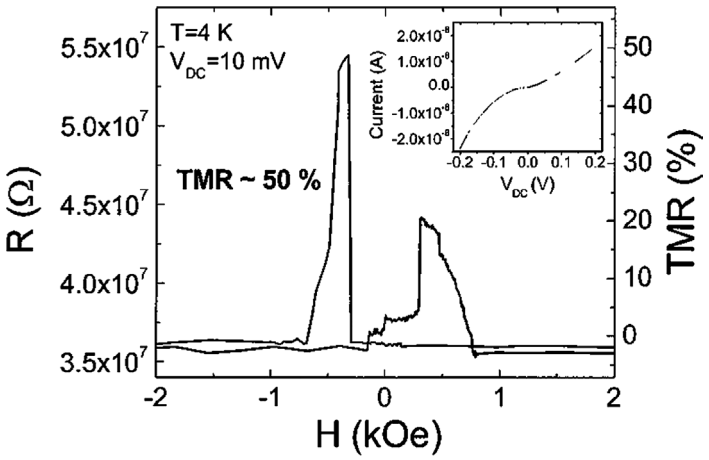

Fig. 7. Magnetoresistance curve obtained with a SFMO-based magnetic tunnel junction. The large magnetoresistance confirms the strong spin polarization of SFMO double perovskite.

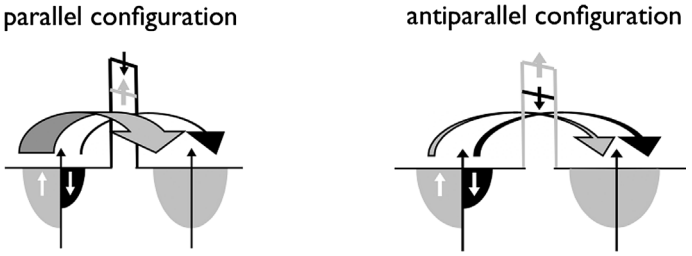

Fig. 8. Schematic structure and operation of a magnetic spin filter.

2.3. Insulating perovskites and spin filtering

An alternative way to obtain magnetoresistive structures is to make magnetic tunnel junctions with an insulating magnetic barrier. In that case, the so-called spin filter structure, initially proposed by Moodera [41], is represented in Fig. 8. The spin-filter structures takes advantage of the difference of barrier height, caused by exchange splitting of the conduction band of the ferro- (or ferri-)magnetic tunnel barrier. Depending on the relative (parallel or antiparallel) magnetic orientations of the magnetic electrode and the tunnel barrier, the current flow through the spin filter will vary. The spin filter efficiency is defined by:

$$\Delta R/R = \frac{2P_{e1}P_{\text{barrier}}}{1 - P_{e1}P_{\text{barrier}}} \tag{2}$$

where P_{barrier} is defined as the normalized difference of spin up and spin down transmission coefficients of the filtering barrier. This 'filter efficiency' depends on the difference of barrier height for ↑ and ↓ spin orientations and the mean barrier height.

The initial material chosen for spin filtering were the Eu chalcogenides [41–43], which have a relatively low Curie temperature (around 18 K). The first result obtained by a magnetic tunnel junction with a magnetic barrier was reported by Le Clair in 2002 with Al–EuS–Gd structure [44]. A tunnel magnetoresistance of 120% was observed at 4 K, yielding a filter efficiency of almost 90% for EuS.

A limited number of works on other materials for spin filters have been presented so far, mainly due to the rareness of materials being at the same time ferromagnetic and insulating. In fact, except rare earth chalcogenides that have low Curie temperatures, only ferrites (see Section 2.4) or some perovskite materials exhibit the required properties. In this last class of materials, we must mention the recent work by Gajek et al. [23]. These authors fabricated $La_{2/3}Sr_{1/3}MnO_3$–$SrTiO_3$(1 nm)–$BiMnO_3$–Au junctions. A thin $SrTiO_3$ layer is inserted between $La_{2/3}Sr_{1/3}MnO_3$ and $BiMnO_3$ in order to magnetically decouple both ferromagnetic materials. Bulk insulating perovskite $BiMnO_3$ has a Curie temperature of 105 K, 3.6 μ_B per Mn atom and is a good dielectric. The maximum magnetoresistance they have reported is ∼50% at low temperature (see Fig. 9), indicating a filter efficiency of 22% for $BiMnO_3$, assuming a 90% spin polarization of the $La_{2/3}Sr_{1/3}MnO_3$–$SrTiO_3$ interface.

Among the potential advantages of $BiMnO_3$, it is in principle possible to grow good quality Si–$BiMnO_3$ or GaAs–$BiMnO_3$ heterostructures since it is a perovskite. This opens perspectives for spintronics applications. The other specificity of $BiMnO_3$ is

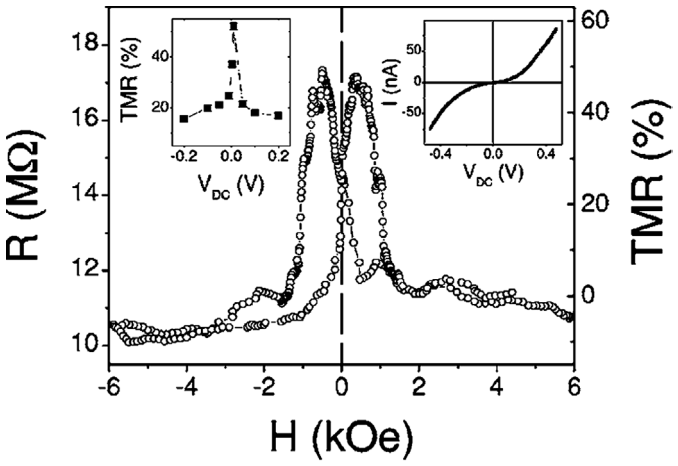

Fig. 9. Tunnel magnetoresistance measured for a $La_{2/3}Sr_{1/3}MnO_3$–$SrTiO_3$(1 nm)–$BiMnO_3$–Au spin filter [23].

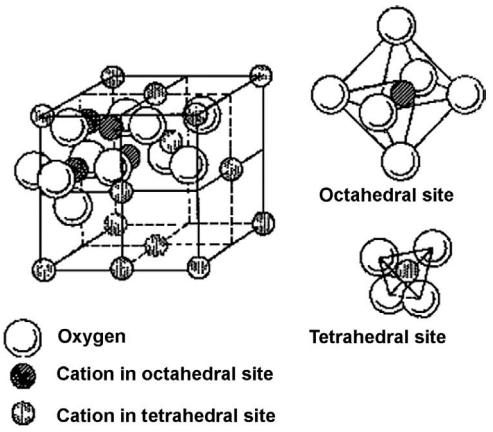

Fig. 10. Schematic structure of one unit cell of the spinel structure (left part) and the interstitial sites of the cations (right part).

that it is at the same time a ferromagnetic material and a ferroelectric material. It is therefore a good candidate for multiferroic applications.

2.4. Ferrites: old materials offering novel applications in spintronics

The spinel ferrites have the chemical formula of XFe_2O_4, where X is a trivalent transition metal ion and the Fe ion is divalent. They constitute a wide group of materials with various physical properties. All of them are insulating in their bulk form, except magnetite Fe_3O_4 which shows conductive behavior at room temperature due to a hopping mechanism. The Curie temperature is typically above room temperature and the magnetic moment is high. But in thin films the research and the application of these materials is still rare, due to the fact that they have a complex crystal structure with a big unit cell and many unoccupied interstitial sites, which makes them hard to synthesize in thin film form with the bulk properties.

The spinel crystal structure can be described as a close-packed face-centered cubic oxygen lattice with cations at the interstitial octahedral and tetrahedral sites (see Fig. 10). The unit cell contains 32 oxygen anions and 24 cations. 8 of the cations are distributed on the 64 available tetrahedral sites (A-sites) and 16 on the 32 available octahedral sites (B-sites). The cations are distributed in that way, that B-site cations form a chain along the [111] direction of the lattice [24].

Considering the distribution of the cations over the two possible sites, three different spinel types have to be distinguished, the ‘normal’, the ‘inverse’ and the ‘mixed’ spinel structure. In the normal spinel structure the trivalent cations are found only on the B-sites, while the divalent cations occupy the A-sites. As Fe^{2+} ions prefer the octahedral sites [25], typically the other extreme is observed, the inverse spinel structure, where the divalent ions occupy half of the B-sites and the trivalent ions are distributed equally over half of the B- and over the A-sites (e.g., $NiFe_2O_4$, Fe_3O_4). The mixed structure is a mixture between the normal and the inverse spinel (e.g., $CoFe_2O_4$, $(Mn,Zn)Fe_2O_4$), which occurs if both ions have a similar site preference.

Ferrites show the collinear ferrimagnetic ordering of the Néel theory [26]. Two ferromagnetically ordered sublattices are formed, one by the ions on the A-sites, one by those on the B-sites. The intersublattice coupling is antiferromagnetic and relatively strong, due to a superexchange interaction between these ions. The intrasublattice coupling between the different ions on B-sites is also a (weak) antiferromagnetic superexchange coupling (except for Fe_3O_4 where the mixed valence of the Fe ions leads to a ferromagnetic double exchange interaction), which is weaker than the interlattice coupling due to the larger distance between the B-site ions. The distance between A-site ions is even larger, and so the weak antiferromagnetic super exchange coupling of the A-site ions and of the B-site ions is covered by the strong intersublattice coupling and the intrasublattice ordering is forced to be ferromagnetic. The Curie temperature (T_C) of the ferrites are typically above 700 K, reflecting the very stable magnetic interaction in this system.

Therefore, the magnetic and transport properties are strongly influenced by the distribution of the ions on the A- and B-sites. As this distribution can change in thin film form and depending on the deposition technique, the properties of the thin films can differ strongly from the bulk properties.

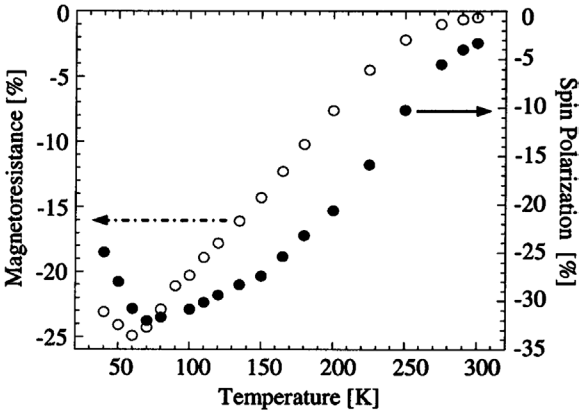

Fig. 11. Junction magnetoresistance (open circles) and deduced spin polarization of Fe_3O_4 (solid circles) as a function of temperature, for a $Fe_3O_4/CoCr_2O_4/La_{0.7}Sr_{0.3}MnO_3$ tunnel junction [31].

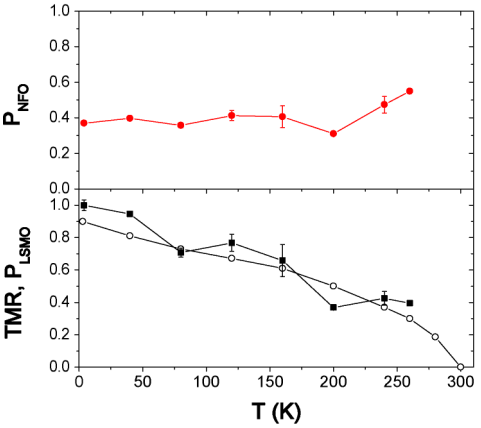

Fig. 12. (Bottom) tunnel magnetoresistance (solid symbols) and the spin polarization of the $La_{0.7}Sr_{0.3}MnO_3/SrTiO_3$ interface (open symbols) vs. temperature for a $La_{0.7}Sr_{0.3}MnO_3/SrTiO_3/NiFe_2O_4$ tunnel junction. (Top) spin polarization of $NiFe_2O_4$ electrode calculated from the TMR ratio [40].

2.4.1. Conductive ferrites

The conductive ferrites are interesting for the application as a source of highly spin polarized currents. Although Fe_3O_4 is not a new material (it was used already by the antique Greeks as a compass) and already quite well understood, the interest in this material was renewed in the recent years when it was predicted theoretically a half-metal [27].

While the full spin polarization was observed experimentally in photoemission experiments [28], experiments with magnetic tunnel junctions showed more disappointing results. Magnetite was used as a magnetic electrode in tunnel junctions [29–32], but the typical spin polarization at low temperature was found to be around 30% which decreases very fastly with increasing temperature until at room temperature a spin polarization of only a few percent is left (see Fig. 11). The same feature was observed by Wei et al. [33], who measured the exchange splitting and the energy gap between majority and minority spins in magnetite. At low temperature they find evidence for half-metallicity, while at room temperature the energy gap between the spin bands was not observable anymore. They discuss that this is maybe due to the Verwey transition observed at 120 K. If the Verwey transition is accompanied by a order–disorder transition, the energy gap would be smeared out due to the disorder. Another intrinsic possibility for the limitation of the spin polarization of magnetite was found by Srinitiwarawong and Gehring [34], they deduce from their calculations that due to the ferrimagnetic ordering and the hopping mechanism 60% will be the highest spin polarization possible. Also the sign of the magnetoresistance is not totally clear. While some groups find a positive magnetoresistance [29,30], others find a negative value [35,31,32,36]. The negative spin polarization is the expected one as band calculations [27] show that magnetite is negatively spin polarized.

Thus, the actually available thin films of Fe_3O_4 show a spin polarization which is comparable to the ferromagnetic metals, but it decreases approaching room temperature. As stated before, the growth of magnetite is extremely complicated, as is the integration of this materials into heterostructures for spintronics. An exact theoretical description of Fe_3O_4 is needed to calculate the intrinsic limit of the spin polarization and its temperature dependence.

Another important issue concerns the possibility to grow epitaxial magnetite films at room temperature in order to integrate such material in semiconductor process. Recent work by Lai et al. [37], who grew magnetite films by ion beam reactive deposition process, have opened the way to such a possibility. These authors obtained good quality Fe_3O_4 films presenting a Verwey transition either on MgO (001) or Si (001) substrates.

While magnetite is the only ferrite which is conductive in its bulk form, recently it was found that thin films of $NiFe_2O_4$ can show conductive behavior, though the bulk material is insulating [38]. The observation of the enhanced conduction was explained by an oxygen deficiency due to the growth of the films in a pure Ar atmosphere. The conductive films were integrated into perovskite heterostructures to build a tunnel junction with $NiFe_2O_4$ as a magnetic electrode [39]. A tunnel magnetoresistance was observed corresponding to a spin polarization of the conductive $NiFe_2O_4$ of up to 40%. Evenmore, the temperature dependence of the magnetoresistance shows that the spin polarization stays constant up to at least 280 K [40] (see Fig. 12).

Thus the modification of the electrical properties of other ferrites by the growth process could lead to a new group of sources of spin polarized current. More work on this topic should lead to insights on the maximum spin polarization possible and on the transport mechanism in this kind of materials.

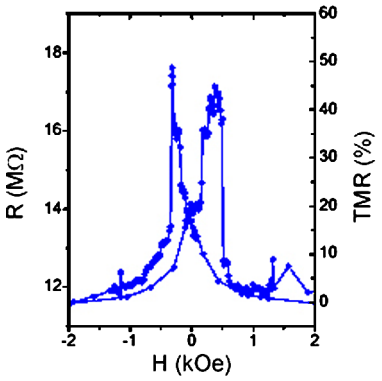

Fig. 13. Resistance vs. field for a $La_{0.7}Sr_{0.3}MnO_3/SrTiO_3/NiFe_2O_4$/Au tunnel junction.

2.4.2. Insulating ferrites

Insulating magnetic materials can be applied in tunnel spin filters, where the exchange splitting of the bands leads to a different barrier height in tunnel junctions and thus a difference in tunnel current for the two spin directions (see Section 2.3). As stated before, most of the ferrites are insulating—and magnetic. As the Curie temperature is typically far above room temperature, these materials are very promising for the application in tunnel spin filter devices. The drawback is the complex crystal structure with indirect magnetic interactions, which could lead to a reduced magnetic moment for very thin films in the range of a few nm required for the use of the film as a barrier.

A tunnel spin filter with a $NiFe_2O_4$ barrier was realized by Lüders et al. [40] with a full spin-polarized LSMO electrode and a Au counterelectrode (see Fig. 13). Although the bulk Curie temperature of the barrier is above room temperature, the observed magnetoresistance diminishes rapidly until at 140 K no signal is observed. However, this is not due to a reduced Curie temperature of one of the two magnetic layers, but due to a coupling as the coercive field of the $NiFe_2O_4$ diminishes with increasing temperature [45].

Thus the results show that it is possible to prepare a magnetic tunnel barrier with the ferrites. This opens a wide field of possible barriers for tunnel spin filters, like $CoFe_2O_4$ with a very high coercive field or $(Ni,Zn)Fe_2O_4$ as a magnetically soft material. Also double spin filters could be envisaged: here the barrier is a hybride barrier of two magnetic insulators, which are magnetically decoupled, and the electrodes are non-magnetic.

3. Diluted magnetic semiconductors

'Making nonmagnetic semiconductors ferromagnetic' [46] may constitute an ultimate stage of intrication for basic spintronic properties. Many efforts have been devoted to the preparation, characterization and understanding of these new materials, of their heterostructures, and of the possible new devices they could allow. Here we briefly review the present achievements of carrier induced ferromagnetism in Diluted Magnetic Semiconductors (DMS).

3.1. What are Diluted Magnetic Semiconductors, and what they are not

Semiconducting ferromagnets, i.e. ferromagnetic materials exhibiting semiconductor-like transport properties, have been known for some time (see a review in [47]). Typical examples are the Europium salts (EuS, EuO) and, more recently, the manganites. In these materials, the ferromagnetic behavior is due to nearest-neighbors spin–spin interactions, even if there is a strong interaction between the carriers in the bands of the semiconductor, and if this interaction gives the opportunity to tune the magnetic properties through the carrier density [48].

The aim of recent studies of Diluted Magnetic Semiconductors is different. The starting point is a normal semiconductor. That implies that:

(1) One can control the transport properties through doping with electrically active impurities. This is the basis of electronics.

However, also, in the context of nanoelectronics, one has to add that:

(2) One can fabricate heterostructures and nanostructures, where combinations of interfaces and electric fields allow one to manipulate the carriers.

Now the goal is that:

(3) The material exhibits ferromagnetic properties which are strongly linked to the carriers in the bands of the semiconductor, so that one can control the magnetic properties through the usual techniques of micro and opto-electronics, and so that the transport characteristics are modified by a change in the magnetic state.

Of course, for applications on a large scale, one has to obtained that:

(4) These properties should be maintained at room temperature and even slightly above, and
(5) All preparation processes should be compatible with fabrication processes used in microelectronics.

Ideally, that means that one should make silicon ferromagnetic at room temperature.

Practically, by substituting the constituent atoms of well-chosen semiconductors with magnetic atoms, some of these five demands have been fulfilled. The main body of results have been obtained with tellurides (PbTe on one hand, II–VI compounds such as CdTe on the other hand) and arsenides (GaAs and other III–Vs). Limited efforts have been devoted to the Si-family (with preliminary reports concerning Ge), and the quest for room-temperature carrier-induced ferromagnetism has motivated significant efforts on wide-bandgap semiconductors such as GaN and ZnO. In most of the cases, the magnetic impurity is Mn, but other transition metals and even rare earths [49] have been tried.

The basic model of carrier induced ferromagnetism is a mean field model [50,51], which is a new version, adapted to the low density of carriers which exists in semiconductors, of a model which appeared unsuccessful to account for the magnetic properties of metals [52]. It describes the consequences of the interaction between free carriers in the conduction band (or the valence band) of the semiconductor, and magnetic impurities. In the absence of interaction, when a field $\boldsymbol{H}$ is applied, the free carriers and the magnetic impurities independently acquire some magnetization. Free carriers obey Fermi–Dirac statistics and their magnetization is given at small field by $\boldsymbol{m}_c = \chi_c \boldsymbol{H}$, where the Pauli susceptibility χ_c is only weakly temperature dependent. Spins localized on the magnetic impurities obey Maxwell–Boltzmann statistics and their magnetization is given at small field by $\boldsymbol{M}_i = \chi_i \boldsymbol{H}$, where the Curie susceptibility χ_i is inversely proportional to the temperature.

In the Zener model of carrier-induced ferromagnetism, the two systems (carriers and localized spins) are described separately as above, and the interaction takes the form of two mean fields. The first one, equal to $\lambda \boldsymbol{M}_i$, describes the effect of the magnetic impurities on the carriers. The large spin splitting it induces (the so-called giant Zeeman effect, proportional to the Mn magnetization [53]) is extremely well documented in II–VI compounds. As a result, the magnetization becomes $\boldsymbol{m}_c = \chi_c(\boldsymbol{H} + \lambda \boldsymbol{M}_i) \approx \chi_c \lambda \boldsymbol{M}_i$ since the giant Zeeman effect is much larger than the direct Zeeman effect. The second mean field, equal to $\lambda \boldsymbol{m}_c$, with the same parameter λ, describes the effect of the carriers on the magnetic impurities. Their magnetization is thus $\boldsymbol{M}_i = \chi_i(\boldsymbol{H} + \lambda \boldsymbol{m}_c)$. Inserting $\boldsymbol{m}_c = \chi_c \lambda \boldsymbol{M}_i$, this becomes $\boldsymbol{M}_i = \chi_i \boldsymbol{H}/(1 - \lambda^2 \chi_i \chi_c)$: the susceptibility measured in the high temperature phase is enhanced by the interaction with the carriers, $\widetilde{\chi}_i = \chi_i/(1 - \lambda^2 \chi_i \chi_c)$. This susceptibility may diverge at a finite temperature T_{CW}. The critical temperature is calculated by inserting the expressions for the Pauli susceptibility χ_c and the Curie susceptibility χ_i. It is proportional to the square of the strength of the spin–carrier interaction (λ^2), to the density of localized spins, and to the Pauli susceptibility of the carriers. If the temperature is decreased below this critical value, the carriers acquire a complete polarization, and the spontaneous magnetization of the impurities continues to increase with a characteristic temperature dependence (upward curvature, [50]).

One main advantage of this model is that it allows one to make comparisons between various compounds [51] or different configurations of the carrier gas (2D or 3D [50]), to introduce the effect of the band structure (e.g., on the anisotropy [54–56]) or of super-exchange spin–spin interactions, to test the coherence from various experimental data including spectroscopy, and so on. Its main drawback is that it assumes that a uniform configuration of the two systems, electronic and magnetic, is achieved, without any influence from disorder. More recent models address the role of disorder [57,58]. They will allow more significant comparisons between theoretical results and experimental data, and should lead to helpful predictions in the quest for room-temperature carrier induced ferromagnetism.

3.2. Ferromagnetism induced by independent carriers

In the periodic table, the series of transition metals corresponds to the progressive filling of the d-shell. A full d-shell corresponds to the column IIb usually involved in the II–VI semiconductors (Zn, Cd, Hg), atoms from column IIa have an empty d-shell (so that Mg has been shown to easily substitute the metal atoms in most II–VIs). Transition metals may also do so, and this is the case of Mn, which enters II–VI compounds as an isoelectronic impurity. The DMSs which result have been extensively studied in the 1970s [59], particularly for their giant magneto-optical effects. Fig. 14 shows, as an example, the position of the reflectance line, as a function of the intensity of an applied magnetic field, observed in a quantum well made of the DMS (Cd,Mn)Te: the Zeeman splitting between the two lines is clearly proportional to the Brillouin function which is

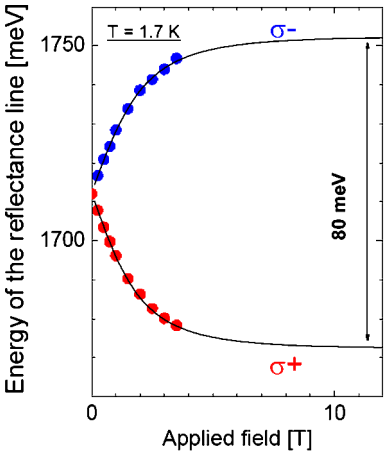

Fig. 14. Giant Zeeman effect measured in reflectivity on a 8 nm thick, $Cd_{0.95}Mn_{0.05}Te$ quantum well with $Cd_{0.65}Mn_{0.08}Mg_{0.27}Te$ barriers, at 1.7 K, in both helicities of light. The solid lines are the fit to the expected shifts, proportional to the magnetization of the Mn system.

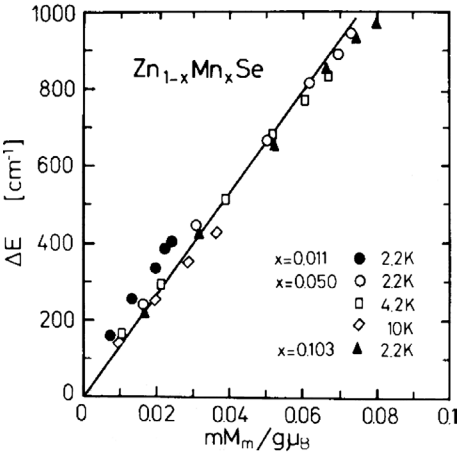

Fig. 15. Giant Zeeman splitting in bulk (Zn,Mn)Se, plotted as a function of the magnetization of the Mn system [60].

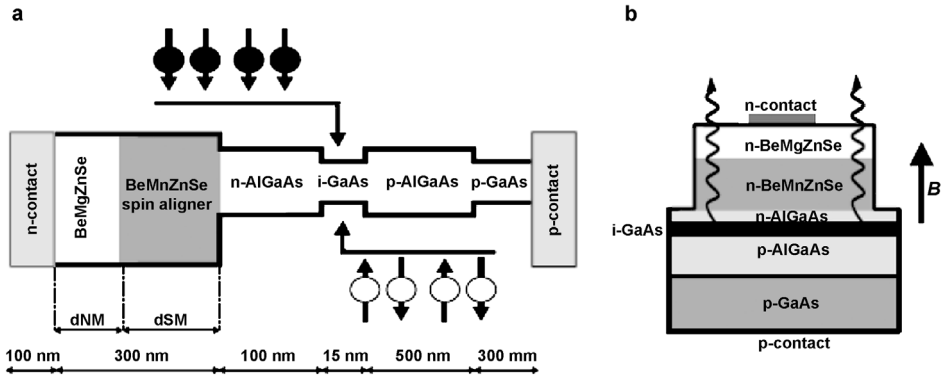

Fig. 16. Device geometry and electric band structure of the spin aligner light-emitting diode. (a) Schematic band structure. Spin-polarized electrons are injected from the left into the active GaAs layer, unpolarized holes from the right. (b) Side view of the device showing the direction of the magnetic field and the emitted light [61].

known to describe the Mn magnetization. Fig. 15 is a compilation of data obtained at various values of the temperature and the applied field, for bulk (Zn,Mn)Se samples [60], which demonstrates the proportionality for a wide range of the Mn content. A large number of studies have focused on the spectroscopy of this class of semiconductors. However, the II–VI semiconductors are usually difficult to dope, and the magneto-optical properties are 'giant' only at low temperature, which restricts a lot the interest of these materials for applications.

More recently, our ability to dope the II–VI semiconductors has improved significantly, so that the range of interest of these materials has been extended to transport. If the material is doped *n*-type, this giant Zeeman splitting induces a strong polarization of the conduction electrons, so that such a material can be used as a spin aligner [61]: the electrons acquire a complete spin polarization in the DMS; they are injected in a non-magnetic structure where they recombine with unpolarized holes, and the helicity of the emitted light measures the spin polarization of the injected electrons (Fig. 16).

The reciprocal effect has been less often demonstrated. In spectroscopy, it should appear as a spin splitting of the Mn due to the presence of the carriers (an effect which is known as the Knight shift for nuclear spins in a metal): such an effect has been detected in a (Cd,Mn)Te quantum well containing a two-dimensional electron gas [62].

The complete effect—carrier induced ferromagnetism—has been achieved in (Pb,Mn)Te, where Mn is also an isoelectronic impurity, and in II–VI compounds like (Zn,Mn)Te and (Cd,Mn)Te quantum wells. In all cases, the ferromagnetic interaction is

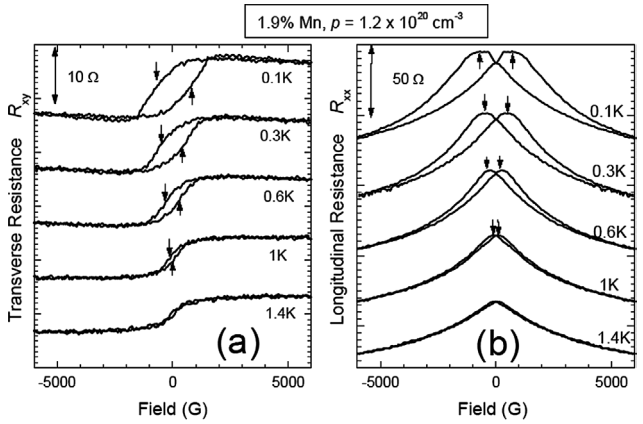

Fig. 17. Hall effect (a) and resistance of a p-doped (Zn,Mn)Te layer [65].

mediated by a large density of holes introduced by doping. We will come back to the two-dimensional case in Section 3.5, and we consider now the 3D case, i.e., bulk samples and epitaxial layers.

In (Pb,Mn)Te, doping was achieved [63] by incorporating Sn. This causes the incorporation of vacancies—which are the electrically active species. Several of the basic properties of carrier induced ferromagnetism have been observed in this system, e.g., the dependence of the magnetic properties on the carrier density, and the influence of the magnetic configuration on the transport characteristics (anomalous Hall effect). Unfortunately, the doping of PbTe is difficult to control, and the incorporation of the ferromagnetic material into nanostructures was not attempted (although beautiful nanostructures are feasible in the PbTe–EuTe system [64]). Hence PbMnTe nicely matches one of the criteria of Section 3.1 (#3), but not the others.

In (ZnMn)Te layers, doping was achieved [65] by incorporating Nitrogen impurities. Actually, ZnTe is the only II–VI semiconductor which can easily be doped p-type, and the efficiency is very high (up to the range of 10^{21} cm^{-3} in layers grown by molecular beam epitaxy and doped with Nitrogen). Carrier induced ferromagnetism was also obtained in bulk (Zn,Mn)Te doped with Phosphorus [66]. Here again, a positive Curie–Weiss temperature was observed in the doped samples (while undoped samples display a negative Curie–Weiss temperature due to superexchange spin–spin interactions), as well as a remanent magnetization (hysteresis). Moreover, these magnetic properties strongly influence the transport properties, such as the magnetoresistance and the anomalous Hall effect (Fig. 17).

Hence (Zn,Mn)Te:N nicely matches the first three criteria:

- the incorporation of the localized spins and the electrically active doping involve different impurities, Mn and N,
- nanostructures can be grown (see also Section 3.5),
- the strong link between magnetic and optical properties (giant Zeeman effect) is observed also on transport properties. Note however that ferromagnetic properties are observed on both sides of the metal-insulator transition [65].

The last two criteria however are not fulfilled (by far, since Curie temperatures are low, a few kelvin only).

3.3. Carrier induced ferromagnetism in the GaAs family

While II–VI DMSs have been known from the early 1970s to easily host magnetic impurities such as Mn, controlling the introduction of Mn into III–V semiconductors such as GaAs appeared to be a more difficult task. For a long time actually, Mn was known as "an undesired contaminant in all III–V semiconductors" [67], particularly in layers grown by molecular beam epitaxy in the early chambers. First attempts to purposely introduce a significant amount of Mn into GaAs or InAs were not totally successful, with a limited amount incorporated into the semiconductor, which was n-type (although Mn was known to be an acceptor when highly dilute in GaAs [67,68]), and antiferromagnetic. Attempts to grow at a more reasonable temperature resulted in the formation of clusters of MnAs [69]. A p-type conductivity was obtained later first in InAs [70], then in GaAs [71], with a clear evidence of the interaction between the carriers and the spins, i.e., between transport properties and magnetization, and the evidence of a ferromagnetic behavior. The success was due to a very low temperature of growth, Fig. 18 [46], with, however, a high suspicion of defects, in particular As antisites. For a long time, the critical temperature appeared to be limited to 110 K; materials with a large Mn content were heavily compensated, although a quantitative determination of the carrier density was made difficult by the very strong anomalous Hall effect. In spite of these difficulties to control the material, these results motivated a strong interest both from experimentalists and theoreticians. The mean field model proved to be surprisingly

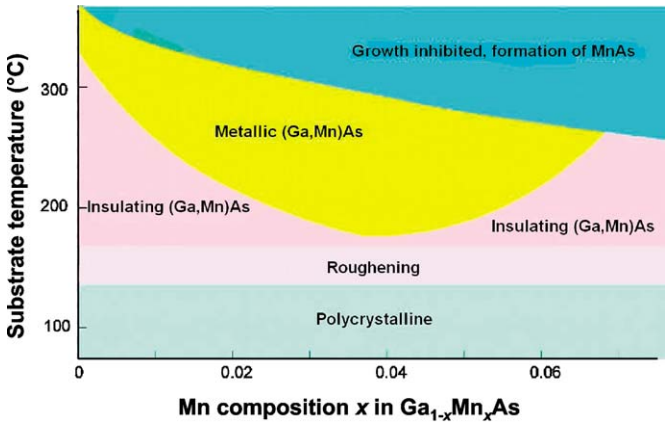

Fig. 18. Schematic phase diagram showing the relation between growth parameters (substrate temperature and Mn concentration) and the properties of (Ga,Mn)As grown by molecular beam epitaxy. The high concentration of Mn in excess of its solubility limit was introduced by nonequilibrium growth at low temperatures [46].

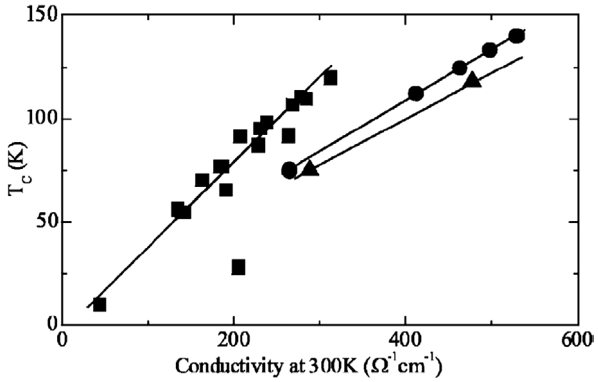

Fig. 19. Curie temperature vs. room temperature conductivity for GaMnAs films with $x = 0.08$ (squares), $x = 0.06$ (circles), $x = 0.05$ (triangles). Straight lines are to guide the eye [80]. No saturation is observed.

successful to account for the dependence of the critical temperature on the carrier density and spin density, and also of the magnetization and its anisotropy on temperature, carrier density and spin density [54].

A step towards a better control of the material was achieved by using post-growth low temperature annealing. The efficiency of annealing drastically depends on the proximity of the surface and on the conditions of annealing. The effect is blocked on thick layers and on capped layers [73,74], and it is sensitive to the conditions at the surface [75,76] and even to nanopatterning [77]. On thin layers close to the surface, the result is both a reduction of the electrical compensation and an increase of the critical temperature [78–80], as shown in Fig. 19. These improvements are ascribed to the outdiffusion of interstitial Mn [81,74], which act as compensating donors and at the same time tend to form antiferromagnetically coupled pairs with the substitutional Mn atoms. As a result, several groups now obtain critical temperatures of the order of 150 K or above [82].

At present, (Ga,Mn)As matches all criteria of the introduction, but one.

(1) Doping GaAs is easy. In (Ga,Mn)As, of course, the conductivity remains p-type; codoping with donors lowers the critical temperature, and co-doping with acceptors has strong limitations [83]. Hydrogen passivates the Mn acceptor, thus suppressing ferromagnetism [84–86]. A conversion to a spin-polarized electron current is achieved in Esaki (Zener) diodes [87,88].
(2) A large variety of heterostructures and nanostructures can incorporate (Ga,Mn)As. Only a part of it will be presented in Section 3.5, others are described in other contributions.
(3) The link between the spin system and the carriers is demonstrated by many observations such as that of a strong anomalous Hall effect [46], the control of the critical temperature and the magnetization when the carrier density is changed (by an electrostatic gate [72] or optically [89]), spectroscopy [90], and so on. . .

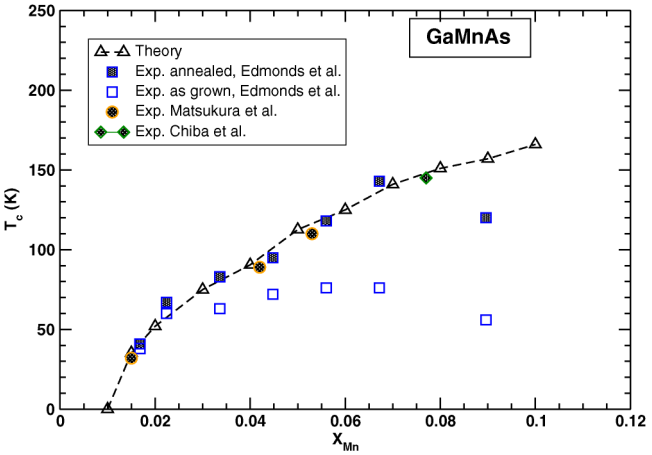

Fig. 20. T_C as a function of doping for $Ga_{1-x}Mn_xAs$: theory for uncompensated samples, and experiment [58].

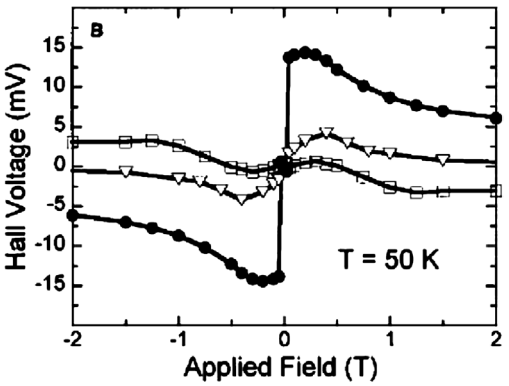

Fig. 21. Hall voltage vs. applied magnetic field at 50 K in a gated Hall bar, where a 60.5 V gate voltage is used to vary the hole density in the $Mn_{0.015}Ge_{0.985}$ active layer. At zero gate voltage (triangles), a small anomalous Hall effect signal is observed. As the hole density in the MnGe layer is enhanced (solid circles) or suppressed (squares) by the gate voltage, the anomalous Hall effect signal and corresponding ferromagnetic order are enhanced or suppressed [94].

(4) The critical temperature is still lower than room temperature. The experimental trend (Fig. 19), as well as an extrapolation of the mean field model towards higher Mn contents, suggest that higher temperatures could be achieved, but this is not confirmed (Fig. 20) by more sophisticated models taking into account the effects of disorder [57,58]. A solution might come from more complex materials or heterostructures where one manipulates the distribution of spins [91] or the localization of the carriers [92], see Section 3.5.

(5) GaAs is of wide use in optoelectronics, but the requirement of a low growth temperature followed by annealing (in the form of a thin layer close to the surface) is a limitation. In spite of that, (Ga,Mn)As is the best material at present to explore semiconductor spintronics.

3.4. The quest for diluted ferromagnetic semiconductors usable for spintronics

Ideally, one should achieve carrier-induced ferromagnetism well above room temperature in a silicon-based DMS. This has motivated experimental efforts in two directions: DMS's based on Si and Ge, and wide band-gap DMSs.

3.4.1. Silicon compatible DMSs

Very few reports have been published on Si-based DMSs. The main difficulty is the formation of silicides—although this opportunity might be turned to an advantage [93].

A controlled introduction of Mn into Ge was more successful (Fig. 21) and attractive reports were published [94,95], showing ferromagnetic properties depending on the Mn content, influencing the transport characteristics and controlled by an electrical bias. More recent studies aim at understanding what is the configuration of the Mn impurity in the Ge host lattice [96], and here again the problem of definite compounds can be a real problem. Recent efforts comprise the study of more complex systems [97] and of possible inhomogeneous distributions of the Mn atoms [98].

3.4.2. Towards room temperature carrier induced ferromagnetism?

There is a lot of interesting experimental work on 'exotic materials', which we will not describe here simply because we chose to consider only materials derived from the most classical semiconductors, with the zinc-blende, diamond or wurtzite structure.

The Zener model of carrier-induced ferromagnetic interactions in diluted magnetic semiconductors predicts that high critical temperatures should be achieved in wide band gap semiconductors, provided several assumptions are satisfied [51]. According to this prediction, *p*-type (Ga,Mn)N would be ferromagnetic above room temperature. This implies however the incorporation of 5% Mn into GaN, substituting Ga, in the form of Mn^{2+} ions, with spin 5/2, together with a large *p*-type doping of the

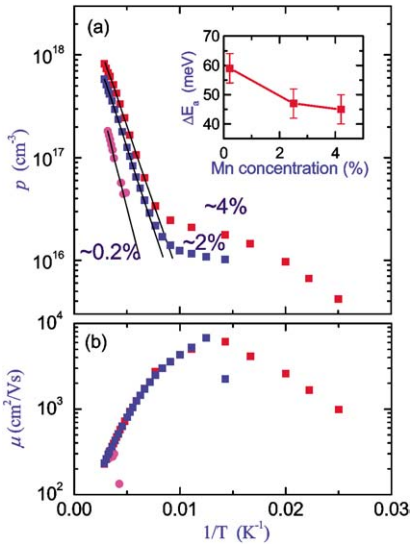

Fig. 22. (a) Hole density, and (b) hole mobility, extracted from Hall measurements, versus temperature for cubic (Ga,Mn)N layers on AlN buffers on GaAs(001), for Mn concentrations 4.2% (filled squares), 2.5% (open squares) and 0.22% (circles). The lines in (a) indicate the fitted curves to the activated hole densities, as described in the text. Inset of (a): acceptor ionization energies extracted from the fits [112].

semiconductor. As we will see, this is very demanding. The same prediction holds for *p*-type (Zn,Mn)O, which has a very similar band structure, and for diamond.

At the same time, ab initio studies [99] indeed suggested that *p*-type (Ga,Mn)N, *p*-type (Zn,Mn)O, but also semiconductors with other transition metal ions, such as (Zn,Co)O, should be ferromagnetic. A few years later, the situation is still very open [100,101]. Early experimental works following this prediction did not give any clearcut conclusion about the magnetic properties of (Ga,Mn)N: ferromagnetic properties at high temperature [102,103] as well as paramagnetic [104] properties down to low temperature, were reported. Several spectroscopic studies contribute to a better understanding of the electronic state of the Mn impurity in GaN. In bulk (Ga,Mn)N with a very low Mn content, the 2+ valence state was detected by electron paramagnetic resonance [105] in agreement with the strong *n*-type character of the samples; in similar samples, the 3+ valence state was deduced from magneto-optical measurements upon co-doping with Mg [106], which is a usual acceptor of GaN. The Mn content in these samples was chosen to be very low, a few 10^{18} cm^{-3} at most, so that a change of the Mn valence can be induced by moderate co-doping with an acceptor such as Mg or a donor such as Si [107]. Various types of valence states, from 2+ to 4+, were invoked to explain optical spectra of epilayers with a larger Mn content[108,109]. An analysis of the X-ray absorption at the K-edge of Mn also points to the 3+ configuration, in spite of an *n*-type conductivity of the samples [110]. Thus, Mn does not behave in GaN as in GaAs, where it forms an acceptor and assumes a 2+ valence state, so that the hypothesis of [51], which is automatically fulfilled in (Ga,Mn)As, cannot be achieved in (Ga,Mn)N, at least in a straightforward way. However, *p*-type conductivity was reported in cubic (Ga,Mn)N layers [111,112], Fig. 22, a very interesting observation which remains to be elucidated and could be extremely useful.

The situation of ZnO is also very controversial. First, some undoped (Zn,Mn)O samples were found to be paramagnetic [113,114], with *n*-type (Zn,Mn)O exhibiting ferromagnetic properties only at very low temperature, in agreement with the mean field model [100]. Others were found to be ferromagnetic [115,116] but this could be due to Manganese oxides [117].

Diverging reports have been published also on (Zn,Co)O. Several groups observed ferromagnetic properties, mainly from magnetization data [113,118–120]. Magneto-optical spectroscopy confirms the spin–carrier coupling [121], without evidence of a zero-field splitting due to the presence of a spontaneous magnetization, and the optical spectroscopy as well as EPR spectra can be explained by independent, anisotropic Co^{2+} spins substituting Zn up to a few % [122,123]. On the other hand, X-ray magnetic circular dichroism at the L2,3 edge of Mn [120], EPR spectra [124] on samples with a higher Co content, and optical MCD in a band below the bandgap [125,126] show evidence of ferromagnetic correlations which tend to increase with the formation of a donor-related band (Fig. 23). Models are invoked which involve a spin–spin interaction through donor species, such as oxygen vacancies [127].

Finally, (Zn,Cr)Te displays not only a magnetization with a ferromagnetic character, but also a strong influence on the magneto-optical spectroscopy [128]. As usual, complementary data reveal that the situation might be more complex [129,130], with strong effects of disorder revealed by field-cooled/zero-field-cooled data. In addition, the magnetic circular dichroism does

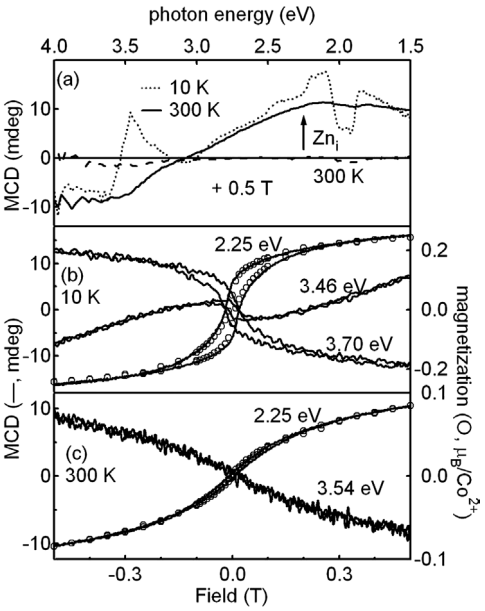

Fig. 23. (a) 300 and 10 K, 0.5 T MCD spectra of 4.2% Co^{2+}:ZnO films. The dashed and solid lines represent before and after exposure to Zn vapor at 450 °C for 1 h in vacuum, respectively. (b) 100 and (c) 300 K magnetic hysteresis loops measured for a 4.2% Co^{2+}:ZnO film exposed to Zn vapor for 1 h at 450 °C. SQUID magnetization data (○) are superimposed upon the MCD data (–).

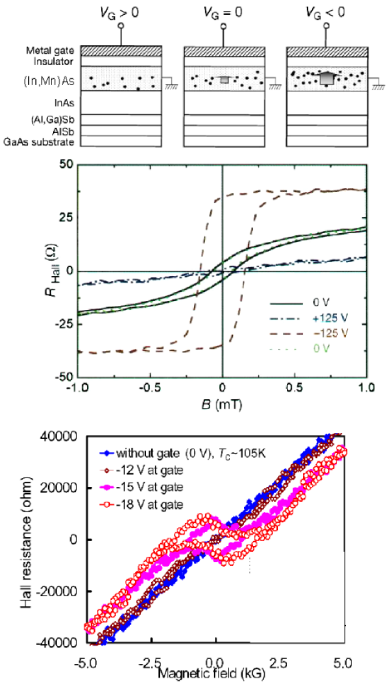

Fig. 24. Progresses in the bias control of carrier induced ferromagnetism in III–V heterostructures; (top) a great achievement: first result in a thin (In,Mn)As layer [72]; (bottom) a more recent result obtained in a modulation-doped (Ga,Mn)As heterojunction [135].

not show a well defined resonance around the gap of the semiconductor [131] but instead features a dichroic structure at lower energy.

3.5. Quantum structures

The growth of quantum structures might offer new ways to control and to enhance the ferromagnetic interactions, as well as new mechanisms and new devices for spintronics. As the second aspect is covered elsewhere in this issue, we focus the rest of this short review to the possibilities of quantum wells and 2D structures, of quantum dots, and of nanowires, towards carrier induced and carrier controlled ferromagnetism.

One major achievement of carrier induced ferromagnetism, is that the paramagnetic–ferromagnetic transition can be crossed, reversibly and isothermally, by changing the carrier density. This was done either optically, or by applying an electrostatic bias in a field effect transistor (FET) structure. In these experiments, it is crucial to work with a rather low areal density of carriers, since this is the main parameter which determines the electric field to be applied. That means either a thin layer of DMS, or a quantum well.

As early (Ga,Mn)As layers did not exhibit ferromagnetic properties if too thin, first results were obtained on (In,Mn)As thin layers. A shift of the critical temperature was induced optically in structures incorporating a (Ga,Al)Sb as a trap [89]. An electric control of ferromagnetism was achieved [72] in a FET structure incorporating a thin (In,Mn)As layer, a (Ga,Al)Sb buffer layer, and a polyimide insulating layer. The change in the magnetic properties was deduced from the anomalous Hall effect. As expected from the large areal carrier density and the large thickness of the insulating layer (0.8 μm), quite a high bias voltage (±125 V) had to be applied in order to shift the critical temperature (Fig. 24). Structures working with a smaller bias voltage were realized later based on (Ge,Mn) [94].

As Mn is an isoelectronic impurity in II–VI compounds, modulation-doped quantum wells can be grown using (Cd,Mn)Te in the well, and (Cd,Mg)Te barriers doped with Nitrogen acceptors. The spontaneous magnetization in the quantum well is deduced [132] from the zero-field splitting of the photoluminescence from the (Cd,Mn)Te (due to the giant Zeeman effect).

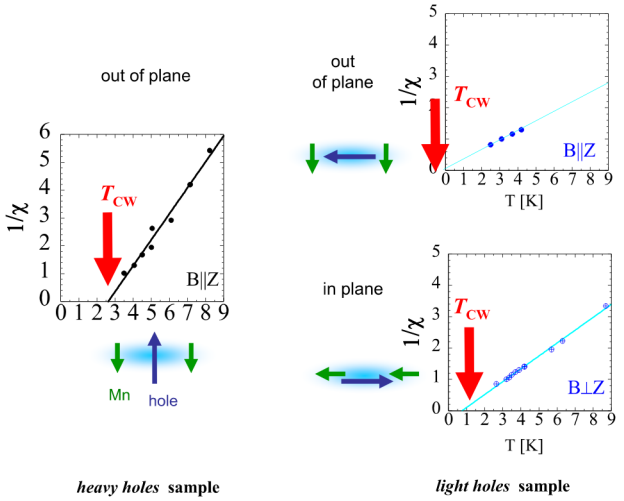

Fig. 25. Manipulation of the magnetic anisotropy in a DMS heterostructure. The susceptibility of a (Cd,Mn)Te quantum well containing heavy holes (which have non-zero spin components along the normal of the quantum well) diverges at positive temperature when the magnetic field is applied out-of-plane (on the left); the susceptibility of a (Cd,Mn)Te quantum well containing light holes (which have small spin components along the normal to the quantum well and larger components in-plane) diverges at positive temperature when the magnetic field is applied in-plane (on the right). Susceptibilities are measured optically [56].

The carrier density in the quantum well is rather low: the average distance between carriers is typically one order of magnitude larger than in (Ga,Mn)As or (Zn,Mn)Te layers [65]. Actually, as long as a single subband is populated, confinement in the quantum well suppresses the Friedel oscillations of the carrier gas in the direction perpendicular to the plane, and a main result is that it cuts the dependence of the critical temperature on the carrier density. In such structures, the magnetic properties can be controlled by a bias voltage as low as 1 V applied across a pin diode, or optically using intrinsic mechanisms governing the recombination of electro-hole pairs photocreated in the barrier [133]. It is also possible to manipulate the anisotropy of the magnetization by a specific design of the quantum well structure (Fig. 25), which takes benefit from the anisotropy of the holes in the valence band [56].

It should be noted also that exchange biasing of (Ga,Mn)As has been realized, particularly with MnO [134].

Modulation-doped (Ga,Mn)As single heterojunctions have been grown more recently and show very encouraging results [135,92,83]. The acceptor, in addition to a plane of Mn (δ-doping), is Beryllium, and it appears that the critical temperature is enhanced if the doped barrier is grown on top of the Mn plane. In the opposite case where the doped barrier is grown first, the formation of interstitial Mn is favored instead, which results in a decrease of the critical temperature. One may note that very high areal densities are obtained (in the 10^{13} cm^{-2} range), which means that several subbands are populated. In spite of that, the carrier density is low enough to allow its manipulation through an electrostatic bias of reasonable value (Fig. 24).

Fewer results have been published on 1D or 0D systems. The case of quantum dots made of a II–VI DMS has been known for some time to exhibit spectroscopic properties related to the formation of a so-called magnetic polaron [136,137]: a magnetic polaron is formed when a carrier (electron, hole) or an electron–hole pair polarizes the localized spins in its neighborhood. The formation of a magnetic polaron has been invoked, too, to explain characteristics of transport through a CdSe quantum dot structure containing Mn spins [138]. At the opposite, a single Mn spin can be localized in a single CdTe quantum dot, and observed by magneto-optical spectroscopy [139]. Some studies of carrier induced ferromagnetism in dots [140] could show a promising way towards room temperature properties.

Finally, it has to be mentioned that the rapidly expanding field of self-organized semiconductor nanowires includes diluted magnetic semiconductors such as (Ga,Mn)N [141,142] and (Zn,Mn)O [143].

3.6. Conclusion

There is still much to do, from the point of view of basic materials science, before Diluted Magnetic Semiconductors can be used on a large scale. Most challenging is the achievement of carrier induced ferromagnetism at room temperature and higher. Simple ideas have proved to be …too simple, but the improvement of our knowledge of this kind of materials and of the mechanisms involved has left several ways open. The study of low dimensional systems—which makes the success of present nanoelectronics—is at its very beginning in the case of carrier induced ferromagnetism.

4. Conclusion

There is presently a strong activity on new materials for spintronics, with the main emphasis on oxydes and semiconductors. The main challenge remains the growth of an ideal material offering a good control of the electronic and magnetic properties and a strong coupling between both, with well mastered interfaces, a critical temperature significantly above room temperature, and a good compatibility with the usual materials and processes of microelectronics. Nevertheless, present materials and heterostructures are sufficiently well controlled that many new basic devices can be imagined and tested. And the subject shows an extremely rapid evolution.

References

[1] V. Goldschmidt, Geochemistry, Oxford University Press, 1958.
[2] A.H. Jahn, E. Teller, Proc. R. Soc. (London) A 161 (1937) 220.
[3] A.H. Jahn, E. Teller, Proc. R. Soc. (London) A 164 (1938) 117.
[4] F. Damay, et al., J. Appl. Phys. 81 (1997) 1372.
[5] L.M. Rodriguez-Martinez, J.P. Attfield, Phys. Rev. B 54 (1996) R15622.
[6] H.Y. Hwang, et al., Phys. Rev. B 52 (1995) 15046.
[7] J.M. de Teresa, et al., Phys. Rev. B 54 (1996) 1187.
[8] W. Prellier, et al., Appl. Phys. Lett. 75 (1999) 1446.
[9] M. Rajeswari, et al., Appl. Phys. Lett. 73 (1998) 2672.
[10] P. Schiffer, et al., Phys. Rev. Lett. 75 (1995) 336.
[11] C.W. Searle, S.T. Wang, Can. J. Phys. 47 (1969) 2703.
[12] J.F. Bobo, et al., J. Appl. Phys. 87 (2000) 6773.
[13] Y. Tomokia, et al., Phys. Rev. B 53 (1996) R1689.
[14] S. Valencia, et al., J. Appl. Phys. 94 (2003) 2524.
[15] A. Gupta, J.Z. Sun, J. Magn. Magn. Mater. 24 (1999) 200.
[16] M. Bowen, et al., J. Appl. Phys. Lett. 82 (2002).
[17] J.H. Park, et al., Phys. Rev. Lett. 81 (1998) 1953.
[18] G. Xiao, et al., J. Appl. Phys. 81 (1997) 5324.
[19] Y. Tomokia, et al., Phys. Rev. Lett. 74 (1995) 5108.
[20] K.I. Kobayashi, et al., Nature 395 (1998) 677.
[21] L. Balcells, et al., Appl. Phys. Lett. 6 (2001) 781.
[22] M. Bibes, et al., Appl. Phys. Lett. 83 (2003) 2629.
[23] M. Gajek, et al., Phys. Rev. B 72 (2005) R020406.
[24] A. Fairweather, et al., Rep. Prog. Phys. 15 (1952) 142.
[25] R.C. O'Handley, Modern Magnetic Materials: Principles and Applications, Wiley-Interscience, 1999.
[26] L. Néel, Ann. Phys. 3 (1948) 167.
[27] R.A. de Groot, K.H.J. Buschow, J. Mag. Mag. Mat. 54 (1986) 2024.
[28] Y.S. Dedkov, et al., Phys. Rev. B 65 (2002) 064417.
[29] X.W. Li, et al., Appl. Phys. Lett. 73 (1998) 3282.
[30] P. Seneor, et al., Appl. Phys. Lett. 74 (1999) 4017.
[31] G. Hu, Y. Suzuki, Phys. Rev. Lett. 89 (2002) 276601.
[32] G. Hu, et al., J. Appl. Phys. 93 (2003) 7561.
[33] J.Y.T. Wei, et al., J. Appl. Phys. 83 (1998) 7366.
[34] C. Srinitiwarawong, G.A. Gehring, J. Phys. Condens. Matter 13 (2001) 7987.
[35] W. Eerenstein, et al., Thin Solid Films 400 (2001) 90.
[36] S. Van Dijken, et al., Phys. Rev. B 70 (2004) 052409.
[37] C.H. Lai, et al., J. Appl. Phys. 95 (2004) 7222.
[38] U. Lüders, et al., Phys. Rev. B 71 (2005) 134419.
[39] M. Bibes et al., in: Proceedings of the 9th International Conference on Ferrites, 2004.
[40] U. Lüders, et al., cond-mat/0508764, submitted for publication.
[41] J.S. Moodera, et al., Phys. Rev. Lett. 61 (1988) 637.
[42] J.S. Moodera, et al., Phys. Rev. Lett. 70 (1993) 853.
[43] T.S. Santos, J.S. Moodera, Phys. Rev. B 69 (2004) 241203.
[44] P. LeClair, et al., Appl. Phys. Lett. 80 (2002) 625.
[45] U. Lüders et al., submitted for publication. See also: U. Lüders: Development and integration of thin spinel oxide films into heterostructures for spintronics, Institut National des Sciences Appliquées de Toulouse, PhD thesis.
[46] H. Ohno, Science 281 (1998) 951.
[47] E.L. Nagaev, Phys. Rep. 346 (2001) 387.

[48] J.B. Torrance, et al., Phys. Rev. Lett. 29 (1972) 1168.
[49] S. Dhar, et al., Phys. Rev. Lett. 94 (2005) 037205.
[50] T. Dietl, A. Haury, Y. Merle d'Aubigné, Phys. Rev. B 55 (1997) R3347.
[51] T. Dietl, et al., Science 287 (2000) 1019.
[52] C. Zener, Phys. Rev. 81 (1950) 440; Phys. Rev. 83 (1950) 299.
[53] J. Gaj, R. Planel, G. Fishman, Solid State Commun. 29 (1979) 435.
[54] T. Dietl, et al., Phys. Rev. B 63 (2001) 195205.
[55] M. Sawicki, et al., Phys. Rev. B 70 (2004) 245325.
[56] P. Kossacki, et al., in: Proc. 11th Int. Conf. on Modulated Semiconductor Structures MSS 11, Nara, 2003; Physica E 21 (2004) 943.
[57] C. Timm, J. Phys. Condens. Matter 15 (2003) R1865.
[58] G. Bouzerar, et al., Europhys. Lett. 69 (2005) 812.
[59] J. Furdyna, J. Appl. Phys. 64 (1988) R29.
[60] A. Twardowski, et al., Solid State Commun. 51 (1984) 849.
[61] R. Fiederling, et al., Nature 402 (1999) 787.
[62] F. Teran, et al., Phys. Rev. Lett. 91 (2003) 077201.
[63] P. Łazarczyk, et al., J. Magn. Magn. Mater. 169 (1997) 151, and ref. therein.
[64] G. Springholz, et al., Appl. Phys. Lett. 62 (1993) 2399.
[65] D. Ferrand, et al., Phys. Rev. B 63 (2001) 085201.
[66] H. Kępa, et al., Phys. Rev. Lett. 91 (2003) 087205.
[67] F. Bantien, J. Weber, Phys. Rev. B 37 (1988) 10111.
[68] J. Schneider, et al., Phys. Rev. Lett. 59 (1987) 240.
[69] H. Munekata, et al., Phys. Rev. Lett. 63 (1989) 1849.
[70] H. Ohno, et al., Phys. Rev. Lett. 68 (1992) 2664.
[71] H. Ohno, et al., Appl. Phys. Lett. 69 (1996) 363.
[72] H. Ohno, et al., Nature 408 (2000) 944.
[73] D. Chiba, et al., Appl. Phys. Lett. 82 (2003) 3020.
[74] K.W. Edmonds, et al., Phys. Rev. Lett. 92 (2004) 037201.
[75] M. Malfait, et al., Appl. Phys. Lett. 86 (2005) 132501.
[76] M. Adell, et al., Appl. Phys. Lett. 86 (2005) 112501.
[77] K.F. Eid, et al., cond-mat/0501298.
[78] K.C. Ku, et al., Appl. Phys. Lett. 82 (2003) 2301.
[79] T. Hayashi, et al., Appl. Phys. Lett. 78 (2001) 1691.
[80] K.W. Edmonds, et al., Appl. Phys. Lett. 81 (2002) 4991.
[81] X. Yu, et al., Phys. Rev. B 65 (2002) 201303.
[82] K.W. Edmonds, et al., in: J. Mendez, C. Van de Walle (Eds.), Proc. 27th International Conference on the Physics of Semiconductors, Flagstaff, July 2004, 2005, p. 333.
[83] T. Wojtowicz, et al., Appl. Phys. Lett. 83 (2003) 4220.
[84] M.S. Brandt, et al., Appl. Phys. Lett. 84 (2004) 2277.
[85] S.T.B. Goennenwein, et al., Phys. Rev. Lett. 92 (2004) 227202.
[86] L. Thevenard, et al., cond-mat/0504387.
[87] M. Kohda, et al., Jpn. J. Appl. Phys. 40 (2001) L1274.
[88] E. Johnston-Halperin, et al., Phys. Rev. B 65 (2002) R041306.
[89] S. Koshihara, et al., Phys. Rev. Lett. 78 (1997) 4617.
[90] A.V. Kimel, et al., Phys. Rev. Lett. 94 (2005) 227203.
[91] G. Bouzerar, et al., Appl. Phys. Lett. 85 (2004) 4941.
[92] A.M. Nazmul, et al., Phys. Rev. Lett. 95 (2005) 017201.
[93] N. Manyala, et al., Nature Materials 03 (2004) 455.
[94] Y.D. Park, et al., Science 295 (2002) 651.
[95] S. Cho, et al., Phys. Rev. B 66 (2002) 033303.
[96] S. Picozzi, et al., Appl. Phys. Lett. 86 (2005) 062501.
[97] F. Tsui, et al., Phys. Rev. Lett. 91 (2003) 177203.
[98] J.-S. Kang, et al., Phys. Rev. Lett. 94 (2005) 147202.
[99] K. Sato, H. Katayama-Yoshida, Jpn. J. Appl. Phys. 39 (2000) L555.
[100] T. Dietl, in: J. Mendez, C. Van de Walle (Eds.), Proc. 27th International Conference on the Physics of Semiconductors, Flagstaff, July 2004, 2005, p. 56.
[101] A.H. MacDonalds, Nature Materials 4 (2005) 195.
[102] H. Hori, et al., Physica B 324 (2002) 142.
[103] V.A. Chitta, et al., Appl. Phys. Lett. 85 (2004) 3777.
[104] R. Giraud, et al., J. Magn. Magn. Mater. 272–276 (2004) 1557.
[105] A. Wołos, et al., Phys. Rev. B 69 (2004) 115210.
[106] A. Wołos, et al., Phys. Rev. B 70 (2004) 245202.
[107] T. Graf, et al., J. Appl. Phys. 93 (2003) 9697.

[108] T. Graf, et al., Appl. Phys. Lett. 81 (2002) 5159.
[109] B. Han, et al., Appl. Phys. Lett. 84 (2004) 5320.
[110] A. Titov, et al., Phys. Rev. B 72 (2005).
[111] S.V. Novikov, et al., Semicond. Sci. Technol. 19 (2004) L13.
[112] K.W. Edmonds, et al., Appl. Phys. Lett. 86 (2005) 152114.
[113] K. Ueda, et al., Appl. Phys. Lett. 79 (2001) 988.
[114] X.M. Cheng, et al., J. Appl. Phys. 93 (2003) 7876.
[115] Y.W. Heo, et al., Appl. Phys. Lett. 84 (2004) 2292.
[116] P. Sharma, et al., Nature Materials 2 (2003) 673.
[117] D.C. Kundaliya, et al., Nature Materials 3 (2004) 709.
[118] H.-J. Lee, et al., Appl. Phys. Lett. 81 (2002) 4020.
[119] M. Venkatesan, et al., Phys. Rev. Lett. 93 (2004) 177206.
[120] K. Rode, et al., J. Appl. Phys. 93 (2003) 7676.
[121] K. Ando, et al., Appl. Phys. Lett. 78 (2001) 2700.
[122] W. Pacuski, et al., cond-mat/0508308.
[123] P. Sati et al., in: Proc. 12th International Conference on II–VI Compounds, Warsaw, 2005.
[124] N. Jedrecy, et al., Phys. Rev. B 69 (2004) R041308.
[125] K.R. Kittilstved, et al., cond-mat/0507121.
[126] K.R. Kittilstved, et al., Phys. Rev. Lett. 94 (2005) 147209.
[127] J.M. Coey, et al., Nature Materials 4 (2005) 173.
[128] H. Saito, et al., Phys. Rev. Lett. 90 (2003) 207202.
[129] N. Ozaki, et al., Phys. Stat. Sol. C 1 (2004) 957.
[130] N. Ozaki, et al., Journal of Superconductivity: Incorporating Novel Magnetism 18 (2005) 29.
[131] S. Marcet et al., in preparation.
[132] A. Haury, et al., Phys. Rev. Lett. 79 (1997) 511.
[133] H. Boukari, et al., Phys. Rev. Lett. 88 (2002) 207204.
[134] K.F. Eid, et al., J. Appl. Phys. 97 (2005) 10D304.
[135] A.M. Nazmul, et al., Phys. Rev. B 67 (2003) 241308.
[136] J. Seufert, et al., Phys. Rev. Lett. 88 (2002) 027402.
[137] A.A. Maksimov, et al., Phys. Rev. B 62 (2000) 7767.
[138] C. Gould, et al., cond-mat/0501597.
[139] L. Besombes, et al., Phys. Rev. Lett. 93 (2004) 207403.
[140] Y.F. Chen, et al., J. Vac. Sci. Technol. B 23 (2005) 1376.
[141] Choi, et al., Advanced Materials 17 (2005) 1351.
[142] J.M. Baik, et al., J. Vac. Sci. Technol. B 23 (2005) 530.
[143] R.K. Zheng, et al., Appl. Phys. Lett. 85 (2004) 2589.